Extended Abstracts of the 2006 International Conference on Solid State Devices and Materials, Yokohama, 2006, pp. 472-473

P-2-6

Analyses of Interface Adhesion between Cu and SiCN Etch Stop Layers by Nanoindentation and Nanoscratch Tests

Shou-Yi Chang* and Yu-Shuien Lee

Department of Materials Engineering, National Chung Hsing University
250 Kuo Kuang Rd., Taichung 402, Taiwan
Tel.: +886-4-22857517; Fax: +886-4-22857017; E-mail: shouyi@dragon.nchu.edu.tw

1. Introduction

Cu with low electrical resistivity has been widely used as multilevel interconnects to reduce resistance-capacitance delay [1]. However, mechanical damages of the films, such as interface delamination caused by stresses, polishing or even packaging, severely suppress the yield and reliability of microelectronic devices [2]. Interface adhesion therefore needs to be clarified. Nanoindentation and nanoscratch tests have been applied for the measurement of the mechanical properties of films [3]. They are promising to determine the interfacial adhesion strength [2, 4-5]. Thus in this study, the adhesion strength and delamination behavior of a typical interface between Cu and SiCN etch stop layers are measured using the nanoindentation and nanoscratch tests.

2. Experimental Procedures

A PECVD oxide (PEOX) film of 460 nm thick and a sputtered TaN barrier layer of 50 nm thick and thin Cu seed layer were grown on a 300 mm Si wafer. A Cu film of 0.6 μm thick were then electrochemically plated, and a top PECVD SiCN etch stop layer of 10 or 100 nm thick was deposited to obtain a Si/PEOX/TaN/Cu/SiCN film stack. A UMIS nanoindenter (CSIRO, Australia) with a nanoscratch test module was used to measure the adhesion strength of Cu/SiCN interface. SEM, TEM, and FIB were used to observe the microstructures and delamination morphologies of the film stacks. High-resolution XPS was employed to evaluate film bonding and compositions.

3. Results and Discussion

Fig. 1 shows TEM images of Si/PEOX/TaN/Cu/SiCN film stack. At Cu/SiCN interface, a thin oxide layer was identified due to the residue of native oxide on Cu surface. Fig. 2 shows the element concentrations in the Cu/SiCN layers with depth measured by XPS analyses. On the SiCN surface, a large amount of O was detected due to surface oxidation, while the SiCN interior was mostly composed of Si, C, and N with uniform concentrations. At the interface at depth of 12 nm, Cu concentration increased, and the others dropped. A high O content was found, confirming TEM observation. Fig. 3 shows the XPS analyses and curve fittings of Si^{2p} spectra at Cu/SiCN interface. The interface was mostly composed of Si-C-N, Si-N, and Si-C bonds. However, Si-N-O bond was detected due to the existence of O. Fig. 4 shows the bonding configurations in the Cu/SiCN layers with depth. From SiCN surface to Cu interior, the constructing bonds moved from high to low binding energy. A slight amount of Cu-Si bond was detected just below the interface, indicating the formation of Cu silicide.

Fig. 5 shows the surface morphologies of Cu/SiCN film stack around the indent marks after nanoindentation tests. Nanoindentation introduced localized deformation into the films, resulting in Cu/SiCN interface delamination as confirmed by Fig. 6, the FIB images. Under a load P of 10 mN, slight interface delamination occurred. At loads P higher than 20 mN, severe interface delamination and even SiCN layer chipping were clearly observed. By using the following Eq. (1) [4], the adhesion energy G_c for Cu/SiCN interface delamination was obtained as about 1.2 J/m^2.

$$G_c = \frac{0.627H^2h\left(1-\nu_f^2\right)}{E_f}\frac{1}{\left[1+\nu_f+2\left(1-\nu_f\right)Ha^2/P\right]^2} \quad (1)$$

where H, h, E_f, and ν_f are the hardness, thickness, modulus and Poisson's ratio of SiCN, and a the delamination length.

Fig. 7 shows the surface morphologies of Cu/SiCN film stack along the scratch tracks after nanoscratch tests. Under sufficient stresses, Cu/SiCN interface delamination and even SiCN layer chipping were observed. The critical load, P_c, for delamination was defined from the variation of load and penetration depth in curves as shown in Fig. 8. By using Eq. (2), the critical stress σ_c for Cu/SiCN interface delamination was obtained as about 2.6 GPa [2, 5].

$$\sigma_c = \left(\frac{2P_c}{\pi d_c^2}\right)\left[\frac{(4+\nu_f)3\pi\mu}{8}-(1-2\nu_f)\right]^2 \quad (2)$$

in which d_c and μ are the critical track width and friction coefficient. By Eq. (3), the adhesion energy for Cu/SiCN interface delamination was obtained as about 1.4 J/m^2 [2, 5], consisting with the value obtained by nanoindentation test.

$$G_c = \frac{\sigma_c^2 h}{2E_f} \quad (3)$$

Acknowledgements

The authors gratefully acknowledge the providence of test wafers by the Taiwan Semiconductor Manufacturing Company.

References

[1] P.C. Andricacos, C. Uzoh, J.O. Dukovic, J. Horkans, and H. Delogianni, IBM J. Res. Develop. **42** (1998) 567.
[2] A.A. Volinsky, N.R. Moody, and W.W. Gerberich, Acta Mater. **50** (2002) 441.
[3] W.C. Oliver and G.M. Pharr, J. Mater. Res. **7** (1992) 1564.
[4] A.A. Volinsky, J.B. Vella, and W.W. Gerberich, Thin Solid Films **429** (2003) 201.
[5] S.J. Bull, Surface and Coatings Technol. **50** (1991) 25.

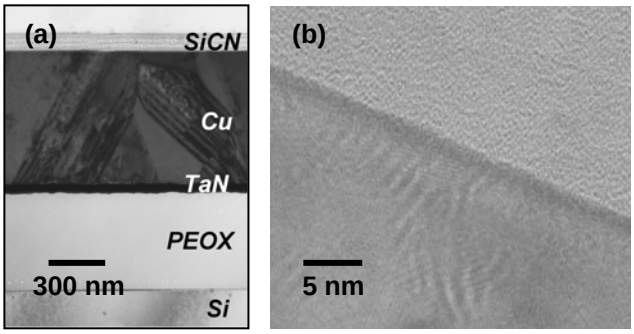

Fig. 1 TEM images of (a) Si/PEOX/TaN/Cu/SiCN film stack and (b) Cu/SiCN interface.

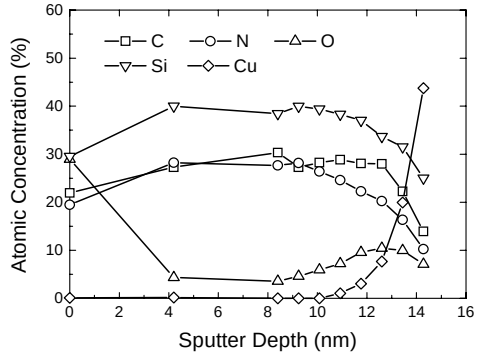

Fig. 2 Element concentrations in Cu/SiCN film stack with depth measured by XPS analyses.

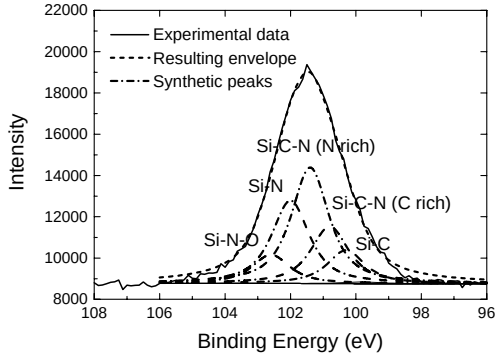

Fig. 3 XPS multiplex analyses and curve fittings of Si^{2p} spectra at the interface of Cu/SiCN film stack.

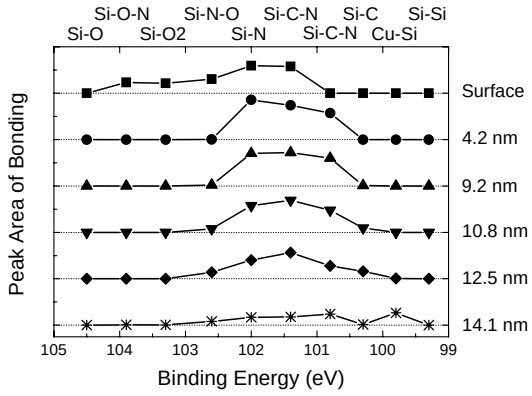

Fig. 4 Bonding configurations in Cu/SiCN film stack with depth measured by XPS analyses.

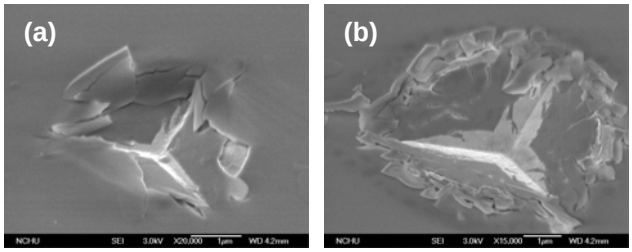

Fig 5 SEM morphologies of Cu/SiCN interface delamination around indents after nanoindentation tests at (a) 20 and (b) 50 mN.

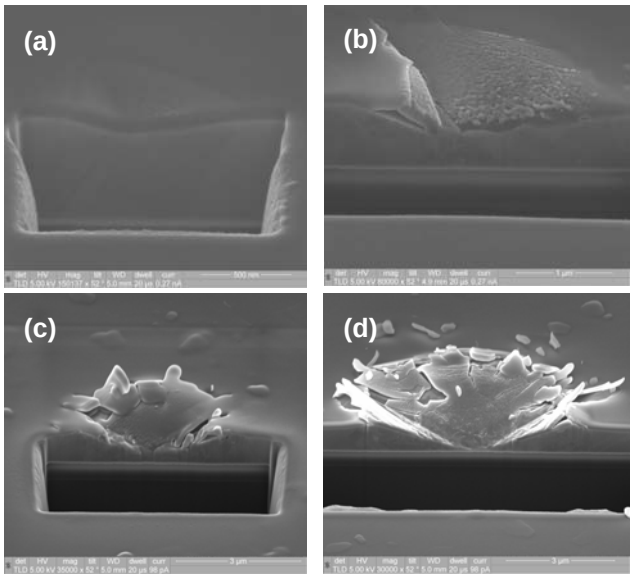

Fig. 6 FIB images of Cu/SiCN interface delamination around indents after nanoindentation tests at (a) 1, (b) 10, (c) 20, and (d) 50 mN.

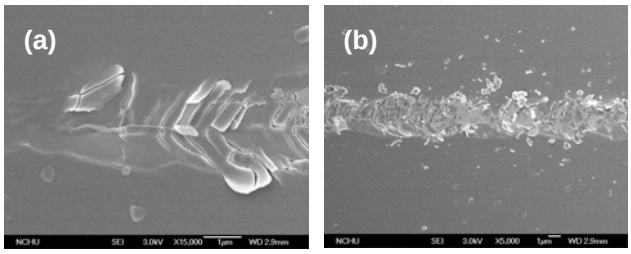

Fig. 7 SEM scratch morphologies at the (a) beginning and (b) late stages of Cu/SiCN interface delamination after nanoscratch tests.

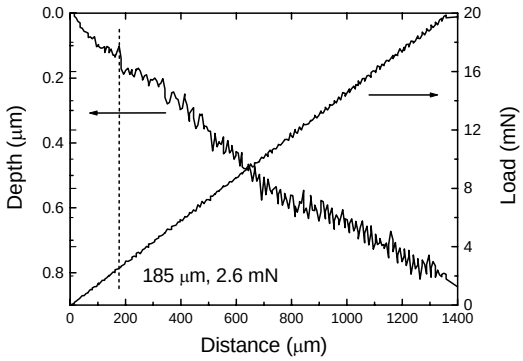

Fig. 8 Typical load-displacement and depth-displacement curves of nanoscratch tests.